Remote Sensing of Autumn Phenology by Including Surface Soil Temperature: Algorithm Development, Calibration, and Validation

Huanhuan Yuan, Xiaoyue Wang [iD], Rachhpal S. Jassal [iD], Linlin Lu [iD], Jie Peng, and Chaoyang Wu

Abstract—Phenology exercises a critical control on annual terrestrial ecosystem carbon uptake and indicates interaction between climate and vegetation. Solely vegetation index is insufficient to accurately detect the end of growing season (EOS). Soil temperature (T_s) plays a modulating role in soil microbial functioning and plant growth, while its impact on EOS remains largely unknown. Hence, we compared the potential between T_s and air temperature (T_a) as the indicators of EOS by using flux data from 14 deciduous broadleaf forests, 24 evergreen needleleaf forests (ENF), 7 mixed forests, and 23 nonforests over Northern temperate and boreal regions (30°–60°N) for 2001–2014. The widely used NDVI-based double-logistic approach failed to capture EOS variability for these ecosystems, and we derived a new EOS algorithm with a soil temperature-based scaler, which improved the EOS modeling for all plant functional types. We found that T_s at different depths showed varied abilities for EOS modeling, and T_s at the 0–10 cm depth provided the best estimates of EOS in terms of both numbers of significant sites and the correlation coefficients (R). Estimated EOS occurred earlier by on average 2.9 days than the current MODIS phenology product for ∼56.5% pixels, especially for the ENF ecosystems (∼5.5 days). Our study suggests the usefulness of surface soil temperature for autumn leaf senescence phenology modeling, and that combination of environmental variables with the current modeling strategy can improve our understanding of autumn phenology with future climate change.

Index Terms—Climate change, end of growing season (EOS), forests, soil temperature.

I. INTRODUCTION

PLANT phenology is of great significance for the understanding of vegetation response to climate change as well as its feedback on the climate system [1]–[3]. Previous studies mainly used solely vegetation indices (VIs) to reconstruct phenological variations [2], [4]–[7]. However, VIs alone are insufficient to accurately detect the date of autumn leaf senescence [i.e., end of growing season (EOS)] [8], [9]. As a result, increasing attempts have been made to improve EOS modeling accuracy by incorporating environmental indicators (e.g., temperature) into the models of EOS to facilitate the capability of the phenological models for a better representation of vegetation productivity [10]–[12].

Remote-sensing technique is the most common and timely approach to detecting large-scale patterns of plant dynamics [3], [13]–[15], and it also serves as a suitable method to monitor plant phenology [16]–[19]. A widely used strategy to extract phenology is to detect the variation in vegetation color (e.g., canopy greenness) [20], [21], and VIs are used as the indicators of phenological transitions [22]–[24]. For example, the normalized difference vegetation index (NDVI) [25], enhanced vegetation index (EVI) [26], green–red vegetation index [27], and normalized difference greenness index [28] are applied in extracting phenological transitions for different land cover types (LCTs), including deciduous broadleaf forests (DBF), evergreen needleleaf forests (ENF), mixed forests (MF), and nonforest (NF) [12], [13], [29], [30]. Besides, a variety of methods, including the threshold-based method [31], [32] and change detection method [16], [33], were proposed to detect phenological variations from VIs time series [16]. However, both methods have limitations in selecting suitable thresholds for VIs time series [31], [34], [35] and detecting the abrupt and rapid increase or decrease at green-up/senescence periods [36], [37]. Furthermore, Zeng et al. [38] suggested that the quality of VIs can also be contaminated by noise (e.g., clouds, snow) and uncertainty of perturbations of environmental factors.

Air temperature (T_a) can be used as an indicator of EOS in many terrestrial ecosystems [39]–[41]. As T_a decreases in late autumn, plant hormone abscisic acid starts to form [42], [43]

TABLE I
RELATIONSHIPS BETWEEN THE REGRESSION COEFFICIENTS OF $\ln(\text{EOS}_{\text{NDVI}} \times T_{\text{SCALE}})$ AND AVERAGE NDVI_{AVE}, SPEI_{AVE}, SM_{AVE}, AND ET_{AVE} OF AUTUMN
(SEPTEMBER–NOVEMBER) FOR PLANT FUNCTIONAL TYPES

IGBP	Coefficient a				Coefficient b			
	NDVI	SPEI	SM	ET	NDVI	SPEI	SM	ET
DBF	NS	**y=195.1x-53.9** **R=0.68**	NS	NS	NS	**y=-634.8x+486.9** **R=0.72**	NS	NS
ENF	NS	NS	NS	**y=1.4x-42.1** **R=0.68**	NS	NS	NS	**y=-12.2x+528.5** **R=0.69**
MF	NS	**y=118.2x-11.6** **R=0.80**	NS	NS	NS	**y=-759.4x+393.9** **R=0.80**	NS	NS
NF	**y=195.1x-53.9** **R=0.68**	NS	**y=235.1x-29.0** **R=0.55**	NS	**y=-1112.4x+588.2** **R=0.69**	NS	NS	NS

DBF, ENF, MF, and NF represent deciduous broadleaf forests, evergreen needleleaf forests, mixed forests, and nonforests, respectively. The bold entities indicate the correlation coefficient is significant at $P < 0.05$. NS means that the relationship between coefficient a or b with environmental factors was nonsignificant.

and chlorophyll degradation occurs [6], [44]–[46]. Therefore, it is a promising method to develop the EOS monitoring algorithm by combing VIs and T_a [47]–[49]. For example, Liu et al. [8] combined MODIS NDVI and land surface temperature (LST) to improve EOS modeling of evergreen needleleaf forests. Zeng et al. [50] incorporated LST, photoperiod, and the wide dynamic range vegetation index to detect corn and soybean phenology. Wang et al. [14] proposed a temperature scale containing temporal and spatial variations of T_a with the two bands EVI2 to estimate leaf unfolding date over China's terrestrial ecosystems.

Apart from T_a, soil temperature (T_s) has a potential impact on regulating plant phenology in autumn. Given that previous studies suggest that T_s is a direct growth environmental regulator for plant roots [51]–[53], which influences soil physical processes (e.g., soil moisture (SM), etc.), it could play an important role in controlling plant growth [54], [55]. For example, O'Connell et al. (2019) demonstrate that the microspatial environmental (e.g., soil temperature, SM) conditions had a great influence on phenology in landscapes with low topographic variation over short distances [56]. However, T_s has rarely been considered in optimizing phenology models and its sensitivity to growth also varies in different LCTs. In light of this, we compared the potential of T_s and T_a for EOS modeling for northern temperate and boreal forests. The depth of T_s was also considered. The objectives of our study were as follows:

1) to compare the potential of T_s and T_a as indictors of EOS of mid–high latitude ecosystems;
2) to derive a new EOS modeling algorithm with T_s;
3) to compare the new EOS algorithm with the standard MODIS phenology products for these ecosystems.

II. MATERIALS AND METHODS

A. Study Sites

In this study, we used observations from 68 flux sites (722 site years in total, https://fluxnet.fluxdata.org; Supplementary Table I). All selected sites had at least five years of continuous observations during 2001–2014 and span a latitude range of 30°N–60°N, and longitudinal extent of 130°W–40°E [see Fig. 1(a)]. Mean annual temperature (MAT) and precipitation across the study sites ranged from −14.3 to 22 °C and 0 to 1651 mm, respectively, from 2001 to 2014 [see Fig.1(b)]. We used Version 6 MCD12Q1 LCT1 annual International Geosphere–Biosphere
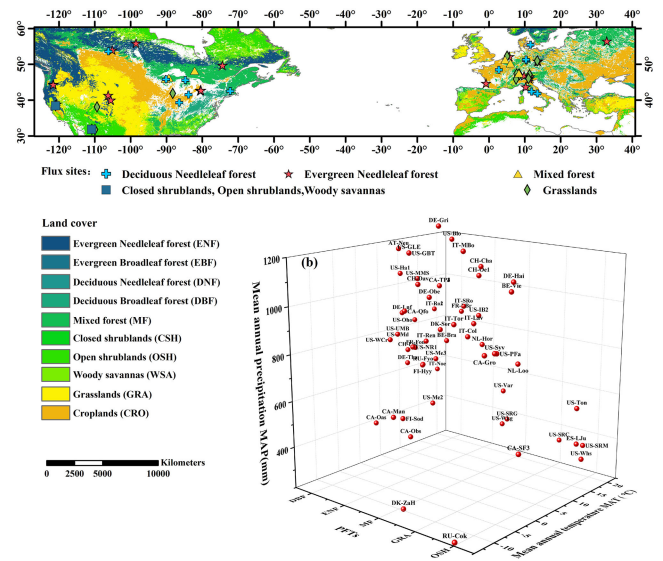

Fig. 1. (a) Spatial distribution of study flux sites used in this analysis. (b) Represents the MAT, total annual precipitation, and LCTs for these sites.

Programme (IGBP) classification in 2010 to classify the LCT of study areas [57]. Croplands' areas are excluded from our study areas because the phenology in these areas is severely affected by human activities. There are 14 DBF sites, 24 evergreen needleleaf forests (ENF) sites, 7 MF sites, and 23 NF sites (especially refers to grasslands, open shrublands, woody savannas, and closed shrublands LCTs) sites.

B. EOS From Flux and Remote-Sensing Data

Phenological data from both site observations and remote-sensing-based phenology were used in our study. Daily GPP data, estimated using the eddy covariance (EC) technique and obtained from FLUXNET 2015 dataset, was used to extract EOS [58]. Daily GPP data of FLUXNET2015 was generated from parting net ecosystem exchange into GPP and ecosystem respiration (Re) [59]. For outlier values (e.g., abnormal high or low GPP values), we used a modified Savitzky–Golay filter (i.e., filter window of 25 and polynomial fit of order 2) to smooth out them from the daily GPP time series [60]. Then, we used a seven-parameter logistic function [i.e., (1)] to fit the daily GPP time series. Finally, we detect the minimum change rate of GPP
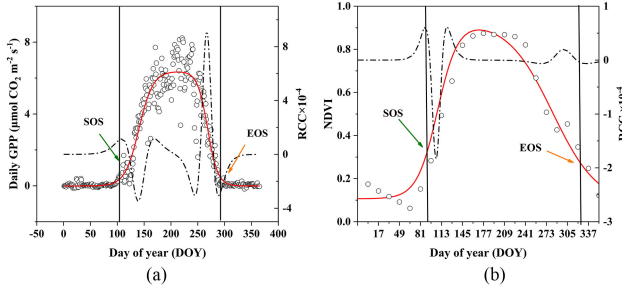
Fig. 2. Schematic representation for calculating the end of growth season using (a) daily GPP from flux sites and (b) 16-day NDVI product from MODIS at CA-Obs site in 2001. DOY represents the day of year. RCC represents the rate of change of curvature.

change rate of curvature [see Fig. 2(a)] [16] to extract the EOS of the year, which was later used as the observed EOS (EOS_{GPP}) for model comparison and development [61], [62]

$$f(x) = a_1 + \frac{a_2}{1 + e^{-b_1(x-c_1)}} - \frac{a_3}{1 + e^{-b_2(x-c_2)}} \quad (1)$$

where $f(x)$ was the NDVI data at time x of the year, and a_1, a_2, and a_3 were the parameters of background value, greenup period value, and senescence period value, respectively. While b_1, b_2, c_1, and c_2 represent the slope and median of the greenup period and senescence period, respectively.

Different data fitting, filtering, and extraction methods have a significant impact on the acquisition of vegetation phenological parameters [63], [64]. To avoid the influence of the method on EOS extracting, a similar method was applied to MODIS NDVI data (i.e., MOD14A1 collection 6, 16-day temporal resolution, and 500 m spatial resolution) employing the same (1) for EOS calculation [see Fig. 2(b)]. For each site, we used the mean NDVI of 3×3 pixels center on the flux tower consistent with the article presented in [65]. Moreover, annual average NDVI <0.1 pixels (e.g., rocks and bare soils) and other contaminated NDVI pixels were excluded. For comparison analysis, we further selected the layer "dormancy" of the standard MODIS phenology product (MCD12Q2 C6; 500 m spatial resolution) [66]. Pre-extracting EOS and pixels with noise caused by clouds and snow were processed by using SG filter, discarded pixels annual mean NDVI over 14 years smaller than 0.1, and replaced with the most recent acceptable quality data.

C. Meteorological Data

Meteorological data used in this study included T_a, T_s, SM, evapotranspiration (ET), and standardized precipitation evapotranspiration index (SPEI) for 2001–2015. T_a was measured at each site with flux measurements. Both T_s and SM have been obtained from famine early warning systems network land data assimilation system products with a spatial resolution of $0.1° \times 0.1°$ and monthly temporal resolution at http://disc.gsfc.nasa.gov, including 0–10 cm, 10–40 cm, 40–100 cm, and 100–200 cm deep levels. ET data were estimated through a machine learning approach (model tree ensemble) integrating EC ET and remote-sensing data at $0.1°$ spatial resolution. We acquired the monthly scale and $0.5°$ spatial resolution SPEI

(2001–2014) from the SPEI base v2.5 at Consejo de Investigaciones Cientificas (http://spei.csic.es). For all meteorological data, we resample them to $0.018°$ spatial resolution to fit the flux site footprints. Moreover, T_s, T_a, ET, SPEI, SM, and NDVI in September–November were used in the following analysis.

D. Statistical Analysis Strategy

To further illustrate the building process of the model, we first explored the suitable depth of T_s and compared it with T_a as indicators of EOS for all sites. Then, we used all data (including 722 site years) to derive a T_s-based scaler to adjust EOS modeled from NDVI. Considering differences among plant functional types, EOS was calibrated for each PFT. Finally, we compared EOS modeled with the standard MODIS EOS products to further confirm the difference.

E. Development of the Soil Temperature Scaler

We used a plant temperature constraint factor [T_c, (2), (3)] [67] together with a temporal temperature indicator [T_m, (4)] to derive the T_s-based scaler (i.e., T_{scale})

$$T_c = 1.1814 \times \left[1 + e^{0.3 \times (-T_0 - 10 + T_s)}\right]^{-1}$$
$$\times \left[1 + e^{0.2 \times (T_0 - 10 - T_s)}\right]^{-1} \quad (2)$$

$$T_0 = \max\left\{\frac{PAR \times f_{APRAR} \times T}{VPD}\right\}. \quad (3)$$

T_c represents the plant temperature constraint factor, T_s represents the soil temperature, and T_0 represents the optimum plant growth temperature [68]–[70]. For T_0, we used a value of 16.1 °C, which was the average T_0 across our study sites

$$T_m = T_{mean}/T_{std} \quad (4)$$

where T_{mean} and T_{std} represent the mean value and standard deviation of autumn T_s for each site, respectively.

$$T_{scale} = T_c \times T_m. \quad (5)$$

Finally, scaled EOS (EOS_{scaled}) is calculated as the product of T_{scale} and the EOS modeled from NDVI (6)

$$EOS_{scaled} = EOS_{NDVI} \times T_{scale}. \quad (6)$$

III. RESULTS

A. Impact of Depth of T_s Used for EOS Modeling

We compared the performance of T_s at different depths (i.e., $T_{s0-10cm}$, $T_{s10-40cm}$, $T_{s40-100cm}$, and $T_{s100-200cm}$) with corresponding GPP-based phenology (EOS_{GPP}). Fig. 3 shows the relationships between EOS_{GPP} and T_s at different depths. We found that T_s at 0–10 cm had the highest correlation ($R = 0.35$) with EOS_{GPP} [see Fig. 3(a)] and that R decreased with the increase in depth ($R_{10-40cm} > R_{40-100cm} > R_{100-200cm}$). Distributions of R between different depths of T_s and EOS_{GPP} [see Fig. 3(f)] also showed that T_s at 0–10 cm had the highest potential for monitoring EOS. Also, T_s at 0–10 cm had the largest significant number of sites (10) for all study sites. It should be
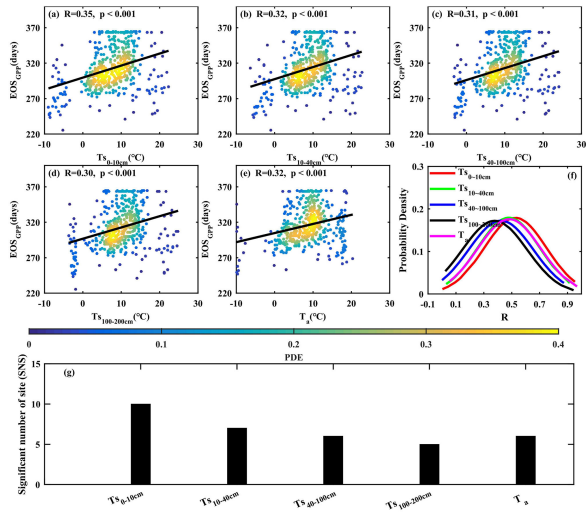
Fig. 3. Relationship between GPP-derived EOS and T_s at different depths (September–November). T_a represents the air temperature. Significant number of sites abbreviated to SNS.
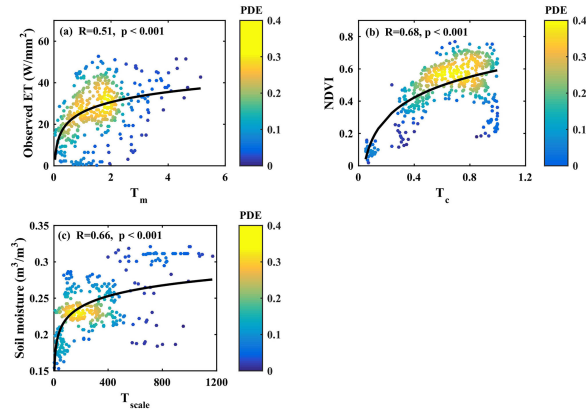

Fig. 4. Relationships among (a) T_m and observed ET, (b) T_c and NDVI, and (c) T_{scale} and SM for all site years. PDE represents the probability density estimate.
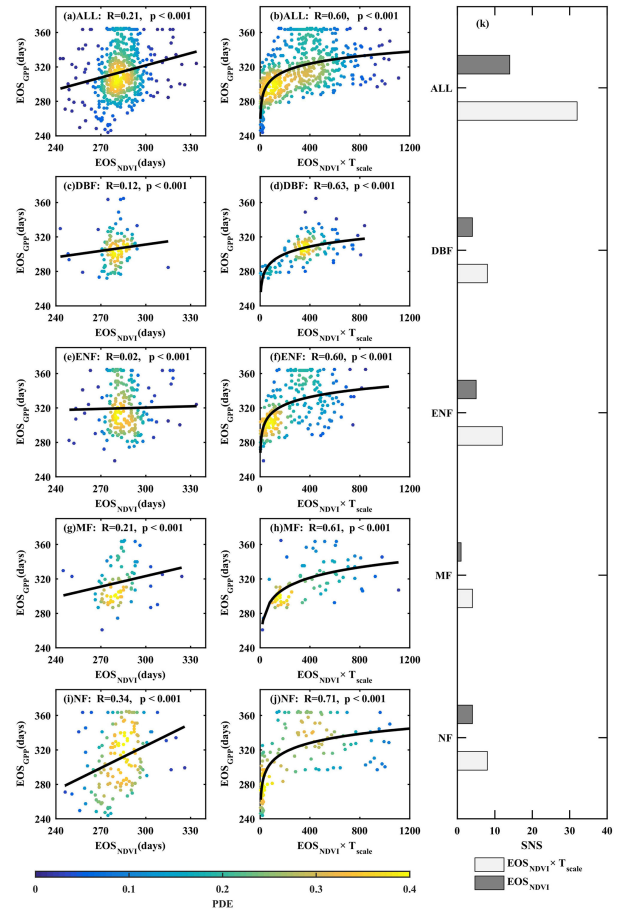

Fig. 5. Relationship between EOS extracted from daily GPP and EOS extracted from double-logistic NDVI (EOS_{NDVI}) for different vegetation types: (a) and (b) all sites, (c) and (d) DBF, (e) and (f) ENF, (g) and (h) MF, and (i) and (j) NF.

noted that $T_{s0–10cm}$ was also a better indicator of EOS than T_a [see Fig. 3(g)].

B. Physical Interpretations of T_{scale}

We investigated the relationships between scale factors (i.e., T_{scale}, T_m, and T_c) and plant growth environmental factors (i.e., ET and SM) across all site years (see Fig. 4). T_{scale} had a significant relationship with SM ($R = 0.66$ and $p < 0.01$), and the components of T_{scale} (i.e, T_m and T_c) also had significant relationships with ET ($R = 0.51$) and NDVI ($R = 0.68$). These results imply that T_{scale} is associated with plant growth status (i.e., NDVI) and environmental conditions, and thus could have the potential to improve the accuracy of EOS estimation.

C. Predictive Capability of $EOS_{NDVI} \times T_{scale}$ in Modeling EOS

To show the predictive capability of $EOS_{NDVI} \times T_{scale}$ (i.e., EOS_{scaled}) in modeling EOS, we compared both EOS_{NDVI} and

EOS_{scaled} with EOS_{GPP}. EOS from NDVI alone (EOS_{NDVI}) seemed to be insufficient to provide reliable estimates of EOS_{GPP} as indicated by a low R of 0.21 for the overall dataset [see Fig. 5(a)]. In comparison, the inclusion of T_{scale} helped to improve the EOS modeling by significantly increasing R to 0.60 [see Fig. 5(b)]. Similar results were also found in each biome type and the modeling performances of greatly improved R are increasing from 0.02 to 0.34 for EOS_{NDVI} to 0.60 to 0.71 and EOS_{scaled} (see Fig. 5). In terms of significant sites, we found that the number of significant sites significantly increased from 14 for EOS_{NDVI} to 32 for EOS_{scaled}. In particular, the largest improvement was found for ENF sites where 12 sites showed significant relationships between EOS_{scaled} and EOS_{GPP}, compared with 5 sites between EOS_{NDVI} and EOS_{GPP} [see Fig. 5(k)].

D. Parameterization of Empirical EOS Model for Different Biomes

Given the nonlinear relationship between EOS_{GPP} and EOS_{scaled}, we then estimated EOS_{scaled} as follows:

$$EOS_{scaled} = a_i \times \ln\left(EOS_{NDVI} * T_{scale}\right) + b_i. \qquad (7)$$
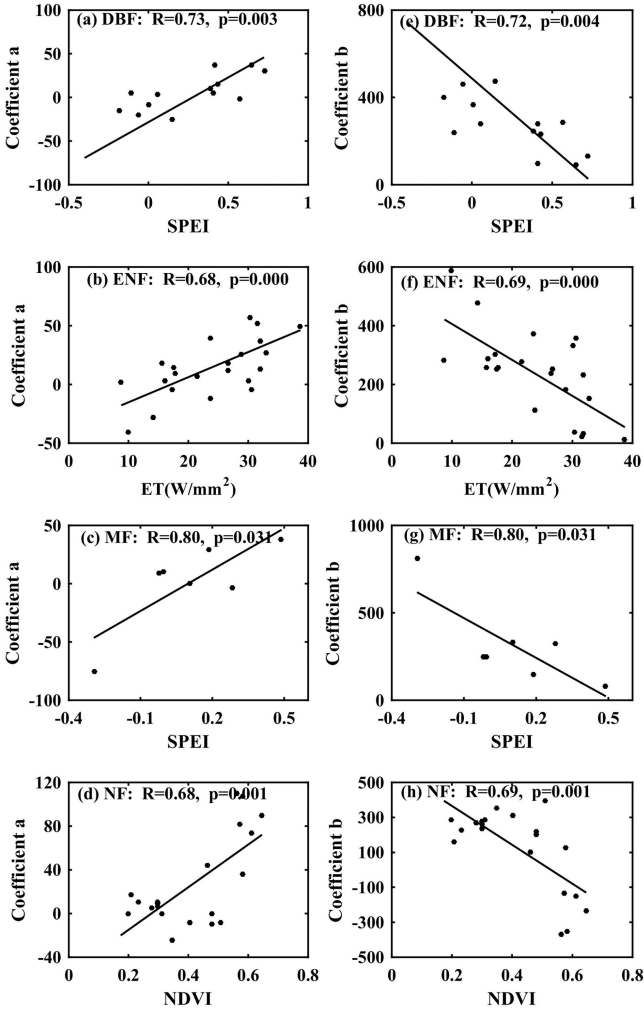
Fig. 6. Model calibration using variables for each LCT. (a)–(d) represent estimating coefficient a using site-specific variables for DBF, ENF, MF, and NF sites. (e)–(h) represent estimating coefficient b using site-specific variables for DBF, ENF, MF, and NF sites. The coefficients a and b were the slope and intercept of line regression between the observed EOS and scaled EOS_{NDVI} ($EOS_{scaled} = a \times \ln(EOS_{NDVI} \times T_{scale}) + b$).

The coefficients a_i and b_i responded differently among vegetation types and environmental factors. For DBF and MF, significant correlations ($R = 0.73$, $p < 0.05$ and $R = 0.80$, $p < 0.05$, respectively) [see Fig. 6(a) and (c)] were observed between the coefficient a and average SPEI (i.e., average SPEI during September–November, $SPEI_{ave}$). $SPEI_{ave}$ was also significantly correlated [see Fig. 6(e) and (g)] with coefficient b for DBF and MF sites ($R = 0.72$, $p < 0.05$ and $R = 0.80$, $p < 0.05$, respectively). Meanwhile, the coefficient a and b for ENF had significant relationship ($R = 0.68$, $p < 0.05$) with autumn average ET (i.e., ET_{ave}) [see Fig. 6(b) and (f)]. Moreover, the coefficient a was found to be significantly correlated with both average NDVI (i.e., $NDVI_{ave}$; $R = 0.68$, $p < 0.05$) and average SM (i.e., SM_{ave}; $R = 0.55$, $p < 0.05$) [see Fig. 6(d)] for NF sites. In comparison, only $NDVI_{ave}$ was significantly correlated with coefficient b ($R = 0.69$, $p < 0.05$) [see Fig. 6(h)].

According to the significant relationships between a, b and $SPEI_{ave}$, $NDVI_{ave}$, and ET_{ave} of different biome types, we calculated the average value of the corresponding variables and used equations in Table I to generate coefficients a and b for different biome types. Therefore, the coefficients for the scaled EOS_{NDVI} algorithms were calibrated as follows: Unnumbered Eq. shown at the bottom of the next page, where X represents $\ln(EOS_{NDVI} * T_{scale})$ and EOS_{scaled} represents the predicted EOS. $SPEI_{ave}$, ET_{ave}, and $NDVI_{ave}$ represent the average SPEI, ET, and NDVI of autumn, respectively.

To estimate predictive capability of $EOS_{NDVI} \times T_{scale}$, we compared the EOS_{GPP} with EOS_{scaled} for the overall dataset and each biome using the calibrated equations (see Fig. 7). $EOS_{NDVI} \times T_{scale}$ produced quite promising results for EOS with $R = 60$ and RMSE = 16.5 days for the overall dataset [see Fig. 7(a)]. DBF showed the lowest RMSE (RMSE = 7.9 days), followed by MF (RMSE = 13.1 days).

E. Comparison Between EOS_{scaled} and MODIS EOS

We compared both EOS_{scaled} [see Fig. 8(a)], using 16-day NDVI from MOD13A1 product and $T_{s0-10cm}$, as well as (8), and EOS from yearly MCD12Q2 phenology product (i.e., dormancy layer, $EOS_{MCD12Q2}$) [see Fig. 8(c)]. Overall, the EOS_{scaled} and $EOS_{MCD12Q2}$ were in the range between DOY 210 and 330, with the mean values of 292.7 ± 18.2 DOY and 293.3 ± 36.9 DOY, respectively. For each biome type, the EOS_{scaled} of ENF, DBF, MF, and NF was 292.4 ± 17.7 DOY, 309.5 ± 5.7 DOY, 303.8 ± 16.8 DOY, and 284.2 ± 17.8 DOY, respectively. Correspondingly, the $EOS_{MCD12Q2}$ for each biome was 301.10 ± 36.9 DOY, 308.5 ± 40.1 DOY, 303.2 ± 35.9 DOY, and 279.8 ± 30.5 DOY, respectively. Compared with the current phenology product (MCD12Q2), our EOS_{scaled} had an average advance of 2.9 days than $EOS_{MCD12Q2}$, mainly distributed (56.51%) in the ENF and NF of the study area [see Fig. 8(f)]. In comparison, later EOS was mainly distributed in DBF and MF areas. Further analysis showed that more than 62.6% of the differences were within the range of −7∼7 days [see Fig. 8(g)].

A similar change trend was observed when the average EOS_{scaled} and $EOS_{MCD12Q2}$ at each 0.1° (i.e., six times of spatial resolution 0.018) [see Fig. 8(h) and (i)] and the difference ($EOS_{scaled} - EOS_{MCD12Q2}$) between those two EOS results were overall small. However, the difference considerably changes with biomes; for example, ENF had the highest average difference (−5.5 ± 12.7 days) for about 66.34% of the area where $EOS_{MCD12Q2}$ was larger than EOS_{scaled}.

IV. DISCUSSIONS

A. Importance of Soil Temperature

Soil temperature directly affects the growth of plant roots and the uptake rate of water and nutrients by them, which were indispensable for plant photosynthesis and respiration. Besides, T_s plays a modulating role in plant growth and soil microbial functioning from physiological and ecological perspectives [41], [52], [71]. Consistent with previous studies that T_s variables
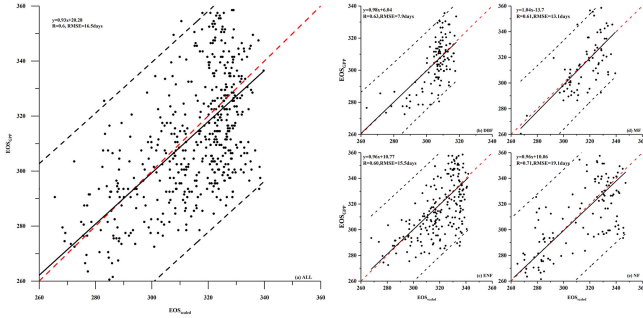
Fig. 7. Comparison between the observed EOS and EOS_{scaled}, including (a) all site-year data, (b) DBF, (c) ENF, (d) MF, and (e) NF. The black dashed lines represent 95% prediction area. The black solid line represents the fitted line. Red dashed lines represent the 1:1 line.

(i.e., temporal variation [8], [14], [72], [73], mean [19], [20], and minimum [5], [74] of T_s) influence vegetation growth, our results demonstrate that T_s plays an important role in improving the accuracy of the EOS modeling. Compared with T_a, T_s at depths below 40 cm (i.e., $T_{s\ 40-100\ cm}$, $T_{s100-200\ cm}$) has relatively lower influence on EOS (see Fig. 3). This is probably because soil temperature varies with daily and annual variation in solar radiation [75]–[77], and the change of soil temperature gradually slowed down in the process of transferring to the deeper soil layer [76]; finally, this change disappeared at a certain depth. Moreover, the time and magnitude of the occurrence of maximum and minimum soil temperature in the deeper layer delay and decrease than surface layer, respectively. Therefore, surface T_s is a complex natural medium that directly or indirectly indicates physical and chemical processes and plant root activity (i.e., absorption of minerals and water as well as respiration), which consequently makes it a better indicator of EOS.

B. Comparison of Mechanisms Between EOS_{scaled} Model and $EOS_{MCD12Q2}$ Model

Compared with EOS_{NDVI} and T_a, our EOS_{scaled} model, based on $EOS_{NDVI} \times T_{scale}$, has better performance in predicting EOS (see Fig. 5). For each biome, the EOS_{NDVI} is greatly improved in ENF and NF [see Fig. 5(c) and (f)] coupling with T_{scale}, and the reason for this may be that the double-logistic NDVI approach requires detectable changes in canopy greenness, while the phenological variations of ENF during autumn were difficult to detect. Furthermore, environmental factors can be helpful in indicating phenology [8], [10], [12], and the T_{scale} has a meaningful connection between environmental conditions [i.e., ET and SM, Fig. 3(a) and (c)] and plant growth parameters [i.e., NDVI, Fig. 3(b)]. As for NF, due to the shallow root system of NFs, changes in surface T_s could be more inclined to cause

direct influences on growth and, thus, a better accuracy of EOS by including T_s.

The comparison between EOS_{scaled} and $EOS_{MCD12Q2}$ for 2015 demonstrates that both EOSs have similar spatial distribution [see Fig. 8(a) and (b)], and the average difference between EOS_{scaled} and $EOS_{MCD12Q2}$ was -2.92 days [62.65% of the study area were within the range of $-7\sim7$ days, Fig. 8(g)]. ENF and NF showed a higher difference between EOS_{scaled} and $EOS_{MCD12Q2}$ than DBF and MF [see Fig. 8(f)], while the percentage of the different areas within -7–7 days in DBF and MF was higher than for ENF and NF. This is mainly because the EOS extracted by Zhang et al. [16] can better indicate the phenological transition of MF and DBF than ENF and NF [8], [22], [45], [78], [79]. Although EOS_{scaled} and $EOS_{MCD12Q2}$ have similar change trends with latitude [see Fig. 8(h) and (i)], the differences were obvious for regions above 55°N. We found that EOS_{NDVI} tends to overestimate EOS of ENF and NF with average values of 5.51 days and 3.56 days than EOS_{scaled}. This agrees with our results in Fig. 5 that, for the overall data, T_{scale} greatly improved the performance of EOS_{NDVI}. Notably, there is a little difference in EOS for DBF between EOS_{scaled} and $EOS_{MCD12Q2}$, which may be the changes in greenness that can be identified more accurately.

C. Limitations of EOS_{scaled} Model

We derived a remote-sensing-based EOS model using a scaled surface soil temperature and a comparison with the standard MODIS phenology product was made for ENF, DBF, MF, and NF vegetation types. Soil temperature is a unique parameter in the surface energy process and regional environmental and climatic circumstances [80], [81]; it can directly or indirectly indicate the habitat of vegetation and circumstances of the root system [82]. Therefore, the EOS_{scaled} model might be more appropriate for estimating EOS by capturing changes in soil temperature. However, the algorithm has limitations when there are large changes in both vegetation EOS and climatic factors in a longer study period because T_{scale}, a_i, and b_i were calculated from the value of September–November and corresponding to the vegetation EOS occurring between Julian days 260 and 340. Second, the model is calibrated using empirical models, and the input parameters are the products of remote-sensing observations or ground measurements, which may impose uncertainties in the operational practice of the algorithm for extreme environments, given the low accuracy caused by these products. While we have shown the applicability of these results for the northern ecosystems, the global application still has challenges. Finally, the improved modeling of EOS needs to be better demonstrated for use in ecosystem models, especially for higher accuracy of modeling of carbon fluxes.

$$EOS_{scaled} = \begin{cases} (102.3*SPEI_{ave} - 28.2) * X + (-634.8*SPEI_{ave} + 486.9) . \ PFT = DBF \\ (1.4*ET_{ave} - 42.1) * X + (-12.2*ET_{ave} + 528.5) . \ PFT = ENF \\ (118.2 * SPEI_{ave} - 11.5) * X + (-759.4 * SPEI_{ave} + 393.9) . PFT = MF \\ (195.1 * NDVI_{ave} - 53.9) * X + (-1112.4 * NDVI_{ave} + 588.2) . PFT = NF \end{cases}$$
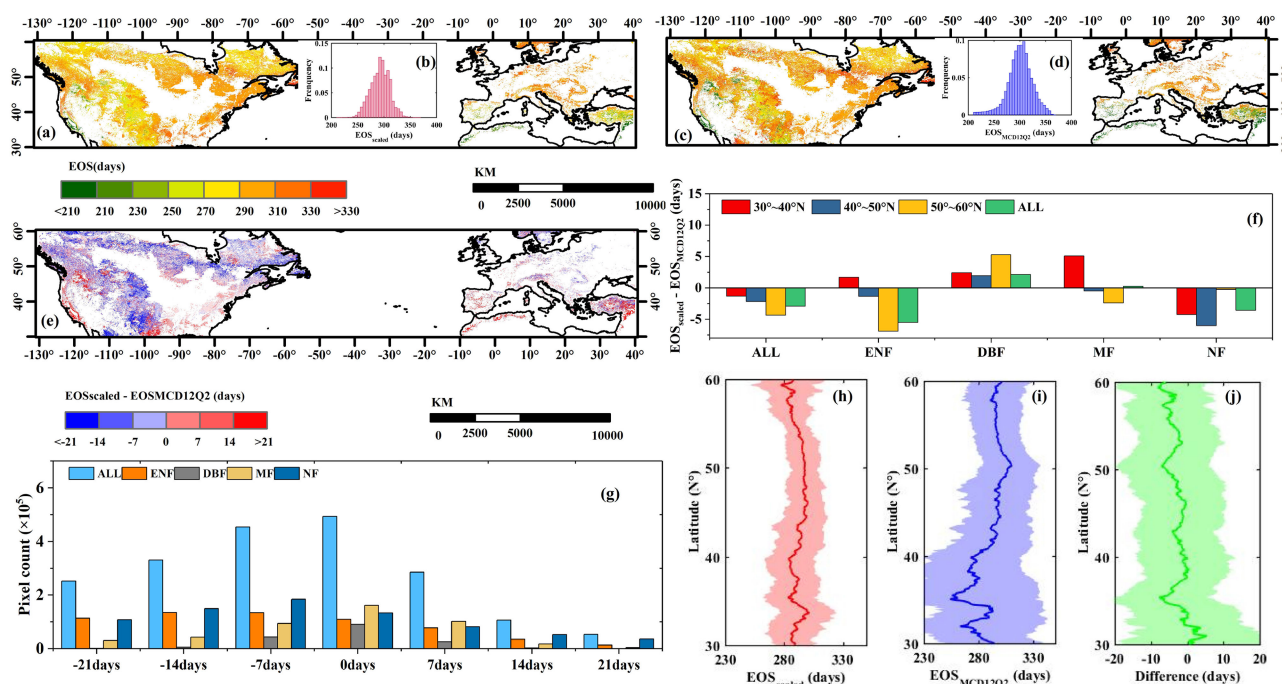
Fig. 8. Spatial distribution of (a) EOS_{scaled} and (c) $EOS_{MCD12Q2}$ over the study area in 2015. (b) and (d) show the frequency distribution of EOS_{scaled} and $EOS_{MCD12Q2}$, respectively. (e) Spatial distribution of EOS_{NDVI} - $EOS_{MCD12Q2}$. Histogram for (f) different latitudes and (g) distribution of EOS_{NDVI} -$EOS_{MCD12Q2}$. (h)–(j) Variation in EOS_{scaled}, $EOS_{MCD12Q2}$, and EOS_{NDVI} - $EOS_{MCD12Q2}$ with latitude. The Shadow represents the standard deviation in each $0.054°$ (i.e., triple of spatial resolution $0.018°$) from $30°N$ to $60°N$.

V. CONCLUSION

Autumn phenology plays an important role in terrestrial ecosystem carbon sequestration. To improve the accuracy of EOS modeling, we used observed EOS at 68 flux tower sites during 2001–2014 over a latitude range of $30°N$–$60°N$ and longitudinal extent of $130°W$–$40°E$, containing ENF, DBF, MF, and NF ecosystems. We found that T_s at 0–10 cm has the best relationship with observed EOS probably because of the major role of soil temperature in regulating plant growth. By incorporating a temperature constraint (T_c), temporal variation (T_m), and canopy greenness change rate date (EOS_{NDVI}), here we proposed a new algorithm of $T_{scale} \times EOS_{NDVI}$ to accurately estimate EOS in various vegetation types. We also used environmental variables to calibrate the model parameters for different biomes and compared EOS modeling with MODIS phenology products in 2015. We observed large regions (56.5%) where MODIS EOS was underestimated. Our results suggest that it would be necessary and promising to consider the role of T_s in future modeling of autumn phenology.

REFERENCES

[1] A. D. Richardson, T. F. Keenan, M. Migliavacca, Y. Ryu, O. Sonnentag, and M. Toomey, "Climate change, phenology, and phenological control of vegetation feedbacks to the climate system," *Agricultural Forest Meteorol.*, vol. 169, pp. 156–173, 2013.

[2] C. Wu et al., "Land surface phenology derived from normalized difference vegetation index (NDVI) at global FLUXNET sites," *Agricultural Forest Meteorol.*, vol. 233, pp. 171–182, 2017.

[3] J. Pastor-Guzman, J. Dash, and P. M. Atkinson, "Remote sensing of mangrove forest phenology and its environmental drivers," *Remote Sens. Environ.*, vol. 205, pp. 71–84, 2018.

[4] H. Jin, A. M. Jonsson, K. Bolmgren, O. Langvall, and L. Eklundh, "Disentangling remotely-sensed plant phenology and snow seasonality at northern Europe using MODIS and the plant phenology index," *Remote Sens. Environ.*, vol. 198, pp. 203–212, 2017.

[5] Y. Wang, Y. Luo, and M. Shafeeque, "Interpretation of vegetation phenology changes using daytime and night-time temperatures across the Yellow River Basin, China," *Sci. Total Environ.*, vol. 693, 2019, Art. no. 133553.

[6] W. Lang, X. Chen, S. Qian, G. Liu, and S. Piao, "A new process-based model for predicting autumn phenology: How is leaf senescence controlled by photoperiod and temperature coupling?," *Agricultural Forest Meteorol.*, vol. 268, pp. 124–135, 2019.

[7] H. M. Kharouba et al., "Global shifts in the phenological synchrony of species interactions over recent decades," *Proc. Nat. Acad. Sci.*, vol. 115, no. 20, pp. 5211–5216, 2018.

[8] Y. Liu et al., "Improved modeling of land surface phenology using MODIS land surface reflectance and temperature at evergreen needleleaf forests of central North America," *Remote Sens. Environ.*, vol. 176, pp. 152–162, 2016.

[9] K. White, J. Pontius, and P. Schaberg, "Remote sensing of spring phenology in northeastern forests: A comparison of methods, field metrics and sources of uncertainty," *Remote Sens. Environ.*, vol. 148, pp. 97–107, 2014.

[10] M. M. Chaves, J. P. Maroco, and J. S. Pereira, "Understanding plant responses to drought - from genes to the whole plant," *Funct. Plant Biol.*, vol. 30, no. 3, pp. 239–264, 2003.

[11] M. Estiarte and J. Penuelas, "Alteration of the phenology of leaf senescence and fall in winter deciduous species by climate change: Effects on nutrient proficiency," *Glob. Change Biol.*, vol. 21, no. 3, pp. 1005–1017, 2015.

[12] Y. Xie, X. Wang, and J. A. Silander, "Deciduous forest responses to temperature, precipitation, and drought imply complex climate change impacts," *Proc. Nat. Acad. Sci.*, vol. 112, no. 44, pp. 13585–13590, 2015.

[13] L. Yu et al., "Monitoring the long term vegetation phenology change in Northeast China from 1982 to 2015," *Sci. Rep.*, vol. 7, no. 1, 2017, Art no. 14770.

[14] J. Wang, C. Wu, X. Wang, and X. Zhang, "A new algorithm for the estimation of leaf unfolding date using MODIS data over China's terrestrial ecosystems," *ISPRS J. Photogramm. Remote Sens.*, vol. 149, pp. 77–90, 2019.

[15] Y. H. Fu et al., "Declining global warming effects on the phenology of spring leaf unfolding," *Nature*, vol. 526, no. 7571, pp. 104–107, 2015.

[16] X. Zhang et al., "Monitoring vegetation phenology using MODIS," *Remote Sens. Environ.*, vol. 84, no. 3, pp. 471–475, 2003.

[17] Q. Liu et al., "Delayed autumn phenology in the northern hemisphere is related to change in both climate and spring phenology," *Glob. Change Biol.*, vol. 22, no. 11, pp. 3702–3711, 2016.

[18] S. Piao et al., "Leaf onset in the northern hemisphere triggered by daytime temperature," *Nature Commun.*, vol. 6, no. 1, 2015, Art. no. 6911.

[19] Y. Yang, H. Guan, M. Shen, W. Liang, and L. Jiang, "Changes in autumn vegetation dormancy onset date and the climate controls across temperate ecosystems in China from 1982 to 2010," *Glob. Change Biol.*, vol. 21, no. 2, pp. 652–665, 2015.

[20] X. Zhang, M. A. Friedl, C. B. Schaaf, and A. H. Strahler, "Climate controls on vegetation phenological patterns in northern mid- and high latitudes inferred from MODIS data," *Glob. Change Biol.*, vol. 10, no. 7, pp. 1133–1145, 2004.

[21] Y. Ryu, G. Lee, S. Jeon, Y. Song, and H. Kimm, "Monitoring multi-layer canopy spring phenology of temperate deciduous and evergreen forests using low-cost spectral sensors," *Remote Sens. Environ.*, vol. 149, pp. 227–238, 2014.

[22] S. Ganguly, M. A. Friedl, B. Tan, X. Zhang, and M. Verma, "Land surface phenology from MODIS: Characterization of the collection 5 global land cover dynamics product," *Remote Sens. Environ.*, vol. 114, no. 8, pp. 1805–1816, 2010.

[23] H. Jin and L. Eklundh, "A physically based vegetation index for improved monitoring of plant phenology," *Remote Sens. Environ.*, vol. 152, pp. 512–525, 2014.

[24] X. Xiao, S. Hagen, Q. Zhang, M. Keller, and B. Moore III, "Detecting leaf phenology of seasonally moist tropical forests in South America with multi-temporal MODIS images," *Remote Sens. Environ.*, vol. 103, no. 4, pp. 465–473, 2006.

[25] C. J. Tucker and P. J. Sellers, "Satellite remote sensing of primary production," *Int. J. Remote Sens.*, vol. 7, no. 11, pp. 1395–1416, 1986.

[26] A. Huete, K. Didan, T. Miura, E. P. Rodriguez, X. Gao, and L. G. Ferreira, "Overview of the radiometric and biophysical performance of the MODIS vegetation indices," *Remote Sens. Environ.*, vol. 83, no. 1/2, pp. 195–213, 2002.

[27] X. Zhang, F. Zhang, Y. Qi, L. Deng, X. Wang, and S. Yang, "New research methods for vegetation information extraction based on visible light remote sensing images from an unmanned aerial vehicle (UAV)," *Int. J. Appl. Earth Observ. Geoinf.*, vol. 78, pp. 215–226, 2019.

[28] R. Nedkov, "Normalized differential greenness index for vegetation dynamics assessment," *Comptes Rendus de l'Académie Des Sci. La vie Des Sci.*, vol. 70, pp. 1143–1146, 2017.

[29] C. Jeganathan, J. Dash, and P. M. Atkinson, "Remotely sensed trends in the phenology of northern high latitude terrestrial vegetation, controlling for land cover change and vegetation type," *Remote Sens. Environ.*, vol. 143, pp. 154–170, 2014.

[30] Z. Liu et al., "Improved modeling of gross primary production from a better representation of photosynthetic components in vegetation canopy," *Agricultural Forest Meteorol.*, vol. 233, pp. 222–234, 2017.

[31] N. Delbart, L. Kergoat, T. L. Toan, J. Lhermitte, and G. Picard, "Determination of phenological dates in boreal regions using normalized difference water index," *Remote Sens. Environ.*, vol. 97, no. 1, pp. 26–38, 2005.

[32] R. B. Myneni, C. D. Keeling, C. J. Tucker, G. Asrar, and R. R. Nemani, "Increased plant growth in the northern high latitudes from 1981 to 1991," *Nature*, vol. 386, no. 6626, pp. 698–702, 1997.

[33] B. C. Reed, J. F. Brown, D. VanderZee, T. R. Loveland, J. W. Merchant, and D. O. Ohlen, "Measuring phenological variability from satellite imagery," *J. Vegetation Sci.*, vol. 5, no. 5, pp. 703–714, 1994.

[34] H. Kobayashi et al., "Latitudinal gradient of spruce forest understory and tundra phenology in Alaska as observed from satellite and ground-based data," *Remote Sens. Environ.*, vol. 177, pp. 160–170, 2016.

[35] B. Tan et al., "An enhanced TIMESAT algorithm for estimating vegetation phenology metrics from MODIS data," *IEEE J. Sel. Topics Appl. Earth Observ. Remote Sens.*, vol. 4, no. 2, pp. 361–371, Jun. 2011.

[36] K. M. de Beurs and G. F. Henebry, "Spatio-temporal statistical methods for modelling land surface phenology," in *Phenological Research*. Dordrecht, The Netherland: Springer, 2009, pp. 177–208.

[37] R. Tateishi and M. Ebata, "Analysis of phenological change patterns using 1982–2000 advanced very high resolution radiometer (AVHRR) data," *Int. J. Remote Sens.*, vol. 25, no. 12, pp. 2287–2300, 2004.

[38] L. Zeng, B. D. Wardlow, D. Xiang, S. Hu, and D. Li, "A review of vegetation phenological metrics extraction using time-series, multispectral satellite data," *Remote Sens. Environ.*, vol. 237, 2020, Art. no. 111511.

[39] N. Delpierre et al., "Modelling interannual and spatial variability of leaf senescence for three deciduous tree species in France," *Agricultural Forest Meteorol.*, vol. 149, no. 6/7, pp. 938–948, 2009.

[40] H. Hanninen and K. Kramer, "A framework for modelling the annual cycle of trees in boreal and temperate regions," *Silva Fennica*, vol. 41, no. 1, 2007, Art. no. 313.

[41] X. Wang et al., "No trends in spring and autumn phenology during the global warming hiatus," *Nature Commun.*, vol. 10, no. 1, 2019, Art. no. 2389.

[42] S.-J. Jeong and D. Medvigy, "Macroscale prediction of autumn leaf coloration throughout the continental United States," *Glob. Ecol. Biogeogr.*, vol. 23, no. 11, pp. 1245–1254, 2014.

[43] R. B. Primack, H. Higuchi, and A. J. Miller-Rushing, "The impact of climate change on cherry trees and other species in Japan," *Biol. Conserv.*, vol. 142, no. 9, pp. 1943–1949, 2009.

[44] M. Archetti, A. D. Richardson, J. O'Keefe, and N. Delpierre, "Predicting climate change impacts on the amount and duration of autumn colors in a New England forest," *Plos One*, vol. 8, no. 3, 2013, Art. no. e57373.

[45] M. A. Friedl et al., "MODIS collection 5 global land cover: Algorithm refinements and characterization of new datasets," *Remote Sens. Environ.*, vol. 114, no. 1, pp. 168–182, 2010.

[46] S. I. Rosenthal and E. L. Camm, "Effects of air temperature, photoperiod and leaf age on foliar senescence of western larch (Larix occidentalis Nutt.) in environmentally controlled chambers," *Plant, Cell Environ.*, vol. 19, no. 9, pp. 1057–1065, 1996.

[47] L. Liang, M. D. Schwartz, and S. Fei, "Validating satellite phenology through intensive ground observation and landscape scaling in a mixed seasonal forest," *Remote Sens. Environ.*, vol. 115, no. 1, pp. 143–157, 2011.

[48] E. E. Cleland, I. Chuine, A. Menzel, H. A. Mooney, and M. D. Schwartz, "Shifting plant phenology in response to global change," *Trends Ecol. Evol.*, vol. 22, no. 7, pp. 357–365, 2007.

[49] V. P. Khanduri, C. M. Sharma, and S. P. Singh, "The effects of climate change on plant phenology," *Environmentalist*, vol. 28, no. 2, pp. 143–147, 2008.

[50] L. Zeng et al., "A hybrid approach for detecting corn and soybean phenology with time-series MODIS data," *Remote Sens. Environ.*, vol. 181, pp. 237–250, 2016.

[51] L. M. Moore, W. K. Lauenroth, D. M. Bell, and D. R. Schlaepfer, "Soil water and temperature explain canopy phenology and onset of spring in a semiarid steppe," *Great Plains Res.*, vol. 25, pp. 121–138, 2015.

[52] J. Kath and K. G. Pembleton, "A soil temperature decision support tool for agronomic research and management under climate variability: Adapting to earlier and more variable planting conditions," *Comput. Electron. Agriculture*, vol. 162, pp. 783–792, 2019.

[53] J. Kilpelainen et al., "Root and shoot phenology and root longevity of Norway spruce saplings grown at different soil temperatures," *Can. J. Forest Res.*, vol. 49, no. 11, pp. 1441–1452, 2019.

[54] V. O. Sadras, *Crop Physiology: Applications for Genetic Improvement and Agronomy*. New York, NY, USA: Elsevier, 2009.

[55] F. Shati, S. Prakash, H. Norouzi, and R. Blake, "Assessment of differences between near-surface air and soil temperatures for reliable detection of high-latitude freeze and thaw states," *Cold Regions Sci. Technol.*, vol. 145, pp. 86–92, 2018.

[56] J. L. O'connell, M. Alber, and S. C. Pennings, "Microspatial differences in soil temperature cause phenology change on par with long-term climate warming in salt marshes," *Ecosystems*, vol. 23, no. 3, pp. 498–510, Apr. 2020.

[57] D. Sulla-Menashe, J. M. Gray, S. P. Abercrombie, and M. A. Friedl, "Hierarchical mapping of annual global land cover 2001 to present: The MODIS collection 6 land cover product," *Remote Sens. Environ.*, vol. 222, pp. 183–194, 2019.

[58] D. Baldocchi, "Measuring fluxes of trace gases and energy between ecosystems and the atmosphere—The state and future of the eddy covariance method," *Glob. Change Biol.*, vol. 20, no. 12, pp. 3600–3609, 2014.

[59] A. D. Richardson, A. S. Bailey, E. G. Denny, C. W. Martin, and J. O'Keefe, "Phenology of a northern hardwood forest canopy," *Glob. Change Biol.*, vol. 12, no. 7, pp. 1174–1188, 2006.

[60] J. Chen, P. Jonsson, M. Tamura, Z. Gu, B. Matsushita, and L. Eklundh, "A simple method for reconstructing a high-quality NDVI time-series data set based on the Savitzky–Golay filter," *Remote Sens. Environ.*, vol. 91, no. 3/4, pp. 332–344, 2004.

[61] A. D. Richardson et al., "Influence of spring and autumn phenological transitions on forest ecosystem productivity," *Philos. Trans. Roy. Soc. London, B, Biol. Sci.*, vol. 365, no. 1555, pp. 3227–3246, 2010.

[62] C. Wu, A. Gonsamo, C. M. Gough, J. M. Chen, and S. Xu, "Modeling growing season phenology in North American forests using seasonal mean vegetation indices from MODIS," *Remote Sens. Environ.*, vol. 147, no. 18, pp. 79–88, 2014.

[63] N. Cong et al., "Spring vegetation green-up date in China inferred from SPOT NDVI data: A multiple model analysis," *Agricultural Forest Meteorol.*, vol. 165, pp. 104–113, 2012.

[64] G. Zhang, Y. Zhang, J. Dong, and X. Xiao, "Green-up dates in the Tibetan plateau have continuously advanced from 1982 to 2011," *Proc. Nat. Acad. Sci.*, vol. 110, no. 11, pp. 4309–4314, 2013.

[65] D. A. Sims et al., "A new model of gross primary productivity for North American ecosystems based solely on the enhanced vegetation index and land surface temperature from MODIS," *Remote Sens. Environ.*, vol. 112, no. 4, pp. 1633–1646, 2008.

[66] M. Friedl, J. Gray, and D. Sulla-Menashe, "MCD12Q2 MODIS/ Terra+Aqua land cover dynamics yearly L3 global 500m SIN grid V006. 2019, distributed by NASA EOSDIS land processes DAAC," Accessed on: Dec. 16, 2021. [Online]. Available: https://doi.org/10.5067/MODIS/ MCD12Q2.006

[67] C. S. Potter et al., "Terrestrial ecosystem production: A process model based on global satellite and surface data," *Glob. Biogeochem. Cycles*, vol. 7, no. 4, pp. 811–841, 1993.

[68] J. B. Fisher, K. P. Tu, and D. D. Baldocchi, "Global estimates of the land–atmosphere water flux based on monthly AVHRR and ISLSCP-II data, validated at 16 FLUXNET sites," *Remote Sens. Environ.*, vol. 112, no. 3, pp. 901–919, 2008.

[69] T. June, J. R. Evans, and G. D. Farquhar, "A simple new equation for the reversible temperature dependence of photosynthetic electron transport: A study on soybean leaf," *Funct. Plant Biol.*, vol. 31, no. 3, pp. 275–283, 2004.

[70] S. Wang, A. Ibrom, P. Bauer-Gottwein, and M. Garcia, "Incorporating diffuse radiation into a light use efficiency and evapotranspiration model: An 11-year study in a high latitude deciduous forest," *Agricultural Forest Meteorol.*, vol. 248, pp. 479–493, 2018.

[71] Y. Fan et al., "Does phenology play a role in the feedbacks underlying shrub encroachment?," *Sci. Total Environ.*, vol. 657, pp. 1064–1073, 2019.

[72] M. Peaucelle et al., "Spatial variance of spring phenology in temperate deciduous forests is constrained by background climatic conditions," *Nature Commun.*, vol. 10, no. 1, 2019, Art. no. 5388.

[73] C. P. H. Mulder, D. T. Iles, and R. F. Rockwell, "Increased variance in temperature and lag effects alter phenological responses to rapid warming in a subarctic plant community," *Glob. Change Biol.*, vol. 23, no. 2, pp. 801–814, 2017.

[74] M. Shen et al., "Strong impacts of daily minimum temperature on the green-up date and summer greenness of the Tibetan Plateau," *Glob. Change Biol.*, vol. 22, no. 9, pp. 3057–3066, 2016.

[75] I. Yolcubal, M. L. Brusseau, J. F. Artiola, P. Wierenga, and L. G. Wilson, "12—Environmental physical properties and processes," in *Environmental Monitoring and Characterization*, J. Artiola, I. L. Pepper, and M. L. Brusseau, Eds. New York, NY, USA: Elsevier, 2004, pp. 207–239.

[76] M. M. Al-Kaisi, R. Lal, K. R. Olson, and B. Lowery, "Chapter 1— Fundamentals and functions of soil environment," in *Soil Health and Intensification of Agroecosystems*, M. M. Al-Kaisi and B. Lowery, Eds. New York, NY, USA: Elsevier, 2017, pp. 1–23.

[77] R. H. Waring and S. W. Running, "Chapter 7—Spatial scaling methods for landscape and regional ecosystem analysis," in *Forest Ecosystems: Analysis at Multiple Scales*, 3rd ed. New York, NY, USA: Elsevier, 2007.

[78] G. Hmimina et al., "Evaluation of the potential of MODIS satellite data to predict vegetation phenology in different biomes: An investigation using ground-based NDVI measurements," *Remote Sens. Environ.*, vol. 132, pp. 145–158, 2013.

[79] X. Luo, X. Chen, L. Wang, L. Xu, and Y. Tian, "Modeling and predicting spring land surface phenology of the deciduous broadleaf forest in Northern China," *Agricultural Forest Meteorol.*, vol. 198/199, pp. 33–41, 2014.

[80] Q. Hu and S. Feng, "A daily soil temperature dataset and soil temperature climatology of the contiguous United States," *J. Appl. Meteorol. Climatol*, vol. 42, pp. 1139–1156, 2003.

[81] E. A. Paul and F. E. Clark, "Chapter 7—Dynamics of residue decomposition and soil organic matter turnover," in *Soil Microbiology and Biochemistry*, E. A. Paul and F. E. Clark, Eds. San Diego, CA, USA: Academic, 1989, pp. 115–30.

[82] D. C. Coleman and D. H. Wall, "Chapter 5—Soil fauna: Occurrence, biodiversity, and roles in ecosystem function," in *Soil Microbiology, Ecology and Biochemistry*, 4th ed., E. A. Paul, Ed. New York, NY, USA: Elsevier, 2015, pp. 111–149.

Huanhuan Yuan received the B.S. and M.S. degrees from Henan Polytechnic University, Jiaozuo, China, in 2017, and the Ph.D. degree from the Institute of Geographic Sciences and Nature Resources Research, Beijing, China, in 2020, all in cartographers and geographic information system.

She is currently a Research Assistant with the Nanjing Institute of Environmental Sciences, Ministry of Ecology and Environment, Nanjing, China. Her research interests include satellite-based global change and phenology.

Xiaoyue Wang received the B.S. degree in surveying science from the Xi'an University of Science and Technology, Xi'an, China, in 2013, and the M.S. and Ph.D. degrees in GIS from the Institute of Remote Sensing and Digital Earth, Chinese Academy of Sciences, Beijing, China, in 2016 and 2018, respectively.

He is currently an Associate Professor Fellow with the Institute of Geographic Sciences and Natural Resources Research, Chinese Academy of Sciences, Beijing, China. His research interests include satellite-based vegetation phenology and its responses to climate change.

Rachhpal S. Jassal received the M.S. degree from Punjab Agricultural University, Ludhiana, India, in 1974, and the Ph.D. degree from the University of Oxford, Oxford, U.K., in 1984, both in soil science.

He is currently a Professor with the University of British Columbia, Vancouver, BC, Canada. His research interests include the effect of management and climate change on carbon and water balances and other greenhouse gas (N_2O and CH_4) emissions in different forest stands and agricultural crops.

Linlin Lu received the Ph.D. degree in remote sensing from the Institute of Remote Sensing Applications, Chinese Academy of Sciences (CAS), Beijing, China, in 2009.

From 2009 to 2012, she was an Assistant Professor with the Key Laboratory of Digital Earth Science, Institute of Remote Sensing and Digital Earth (RADI), CAS, Beijing, China. Since 2013, he has been an Associate Professor with the Key Laboratory of Digital Earth Science. She is the author of more than 100 journal articles and conference proceeding papers. Her research interests include image information extraction, image classification and time-series analysis applied to vegetation phenology, and urban environment and urban sustainability.

Dr. Lu was appointed as member of Sino-EU Panel on Land and Soil in 2017. She is a member of Group on Earth Observation Human Planet Initiative and Global Urban Observation and Information Initiative. She presently co-chairs the Urban Environment Working Group in the Digital Belt and Road Program.

Jie Peng received the B.S. degree in geographical information science from Northeast Normal University, Changchun, China, in 2014, and the M.S. and Ph.D. degrees in cartography and geographical information system from the University of Chinese Academy of Science, Beijing, China, in 2017 and 2021, respectively.

Since 2022, she has been a Researcher with the College of Ecology, Lanzhou University, Lanzhou, China. She is the author of nine articles. Her research interests include vegetation/plant phenology, carbon cycle, climate change, remote sensing, and plant hydraulics.

Chaoyang Wu received the B.S. degree in surveying science from the China University of Geosciences, Beijing, China, in 2005, and the Ph.D. degree in GIS from the Institute of Remote Sensing and Digital Earth, Chinese Academy of Sciences, Beijing, China, in 2010.

He is currently a Research Scientist in natural resources with the Institute of Geographic Sciences and Natural Resources Research, Chinese Academy of Sciences. His research interests include satellite-based carbon cycling and phenology.